American Mineralogist, Volume 68, pages 195–213, 1983

Magnetite in the carbonatites from the Jacupiranga Complex, Brazil

JOSE C. GASPAR

Instituto de Geosciências
Universidade de São Paulo
São Paulo, Brazil CEP 05508

AND PETER J. WYLLIE

Department of Geophysical Sciences
University of Chicago
Chicago, Illinois 60637

Abstract

Electron microprobe analyses of magnetites from five carbonatite intrusions (C_1, oldest, to C_5, youngest) constituting the carbonatite plug in the Jacupiranga complex confirm previous results from Jacupiranga giving compositions in the magnesioferrite-magnetite series very close to Fe_3O_4. Magnetites from other carbonatites are similar with somewhat more Ti and less Mg. MgO in Jacupiranga magnetites reaches no more than 10 wt.%. All analyzed grains are zoned, with Fe_3O_4 increasing toward the rim. In magnetites from C_2 to C_5, Fe_2O_3 replacement is mainly by Al_2O_3 and less by TiO_2; in C_1 magnetites TiO_2 replacement is more important. Despite their limited range of compositions, the cores of magnetites in each of the five intrusions are chemically distinct and distinguishable from each other as indicated by projections from within the Cr-free spinel prism, $MgFe_2O_4$–Mg_2TiO_4–$MgAl_2O_4$–Fe_3O_4–Fe_2TiO_4–$FeAl_2O_4$, and a plot of Mn *vs.* Mg. Magnetites from special locations such as dikes, banded reaction zones between carbonatite and jacupirangite, and in intergrowths with pyrite, are chemically related but distinct from the carbonatite magnetites. The systematic chemical variation and zoning of magnetites in the five carbonatite intrusions indicate magmatic origin. Magnetite crystals nucleated throughout the crystallization interval of the carbonatites, but most of them show evidence of marginal resorption. The oldest carbonatite, C_1, was probably derived from a magma somewhat different chemically from those producing carbonatites C_2 through C_5. The precipitation of carbonatite C_2 probably went to completion independently of C_3 through C_5, whereas carbonatites C_3 through C_5 probably were precipitated from successive batches of magma representing a continuum in time and magmatic evolution.

Introduction

Magnetite is a characteristic mineral of nearly all carbonatites, usually as an accessory, but locally as an essential mineral (Heinrich, 1966, p. 182). The magnetite occurs as disseminated euhedra, commonly in flow bands, or as lenses and irregular aggregates. Magnetite is also concentrated in ore rocks which occur as integral parts of the ring complexes. The magnetite crystals are homogeneous, but exsolution of lamellar ilmenites may occur (Prins, 1972; Mitchell, 1978; Boctor and Svisero, 1978).

There are few published analyses of magnetites from carbonatites. Mitchell (1978) and Boctor and Svisero (1978) presented analyses of the magnetites from Jacupiranga. Other analyses have been reported from Oka by Gold (1966) and McMahon and Haggerty (1976, 1979), for zoned magnetites from South African carbonatites by Prins (1972), from Alnö by von Eckermann (1974), and from Sarfartôq, Greenland, by Secher and Larsen (1980). Mitchell (1979) summarized the chemical characteristics of the magnetites from carbonatites as "compositionally very close to pure magnetite" and as members of the magnesioferrite–ulvöspinel–magnetite series". According to Mitchell: "the principal characteristics of carbonatite spinels are the lack of

0003–004X/83/0102–0195$02.00

Cr_2O_3, the low TiO_2 and MgO relative to kimberlite spinel, and commonly high MnO".

The presence of five carbonatite intrusions in a single complex at Jacupiranga, and the continuous outcrop and freshness of the rocks in the quarry, make this an unusual opportunity to sample in detail the mineralogy of a carbonatite complex. In this paper, we present detailed chemical analyses of zoned magnetites from the five carbonatites, and explore the applications of their chemistry for petrogenesis.

The Jacupiranga Complex

The Jacupiranga Complex is one of many alkalic complexes, several containing carbonatites, that occur in the border of the Parana Basin, in the south of Brazil. It is 130 ± 5 m.y. old (Amaral, 1978). According to Ulbrich and Gomes (1981) the Jacupiranga Complex and other nearby complexes of similar ages form the Jacupiranga Province. This province was interpreted by Herz (1977) as the site of a hot spot associated with the first triple junction formed in the area during the initial opening of the South Atlantic ocean.

Geology of the complex

Melcher (1966) presented a geological map of the Jacupiranga alkalic complex. The complex has an oval shape with an area of about 65 km^2, and is intrusive into granodiorites and mica schists which are fenitized for some distance from the complex. It is composed mainly of peridotites, pyroxenites, jacupirangites and ijolites, surrounded by fenites and nepheline syenites. According to Melcher (1966), a peridotitic body was first emplaced in the northern half of the intrusion, and then surrounded by a ring intrusion of pyroxenite. South of this, and partly cutting it, an almost circular jacupirangite plug was intruded, and partly differentiated into a concentric, crescent-shape ijolite body. The carbonatites occupy a central position in the jacupirangite.

The carbonatites

The carbonatite body has steeply outward-dipping contacts with the jacupirangite and, according to Melcher (1966), it was emplaced in two plugs, one partly cutting the other. Detailed mapping by one of us (JCG) has revealed the occurrence of five distinct intrusions of different ages, as shown in Figure 1. The intrusions C_1, C_2 and C_3 comprise a southern group, and C_4 and C_5 comprise a northern

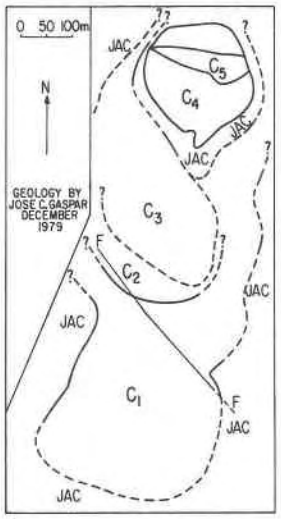

Fig. 1. Simplified geological map of the Jacupiranga carbonatites. C_1—sovite; C_2—dolomitic sovite; C_3—sovite; C_4—sovite; C_5—rauhaugite and JAC—jacupirangite. Solid lines—observed geological contacts; dashed lines—inferred contacts; F—fault. The contacts on the map are incomplete for lack of secure evidence, because the quarry is on a hill.

group. Although the field evidence is not conclusive, it suggests that the southern intrusions are older than the northern intrusions. Given this conclusion, the sequence of carbonatite intrusions from oldest to youngest is C_1, C_2, C_3, C_4 and C_5. The main petrographical and mineralogical features of each carbonatite intrusion are summarized in Table 1.

The intrusive contact of C_3 into C_2 is shown in Figure 1 as a dashed line, because the banding which is obvious within each intrusion becomes diffuse in the region of this contact. In addition, there is an increase in the amount of dolomite present in the rocks near the contact. In some regions, there appear to be a swarm of beforsite dikes intruding the sovites, but in other regions the increase in dolomite could be attributed to a metasomatic process of dolomitization of the sovite. The S and B samples in Table 1 are respectively the calcite and dolomite rock of this region.

Alvikite and beforsite dikes are widely distributed. They usually contain fewer non-carbonated minerals than the larger carbonatite intrusions. The B_4 dike in Table 1 is a beforsite cutting the C_4 sovite. The beforsite dike B_5 is an offshoot from the C_5 rauhaugite, which also cuts the C_4 sovite.

At contacts between carbonatite and jacupirangite (xenoliths and country rock), a banded rock is

Table 1. Petrography of carbonatites and jacupirangite

		Rock type*	Main mineralogy**	Grain size	Other features
Southern Intrusions	C_1	Sovite	Calcite, apatite, magnetite, olivine, phogopite, dolomite, sulfides.	Coarse	Coarsely banded
	C_2	Dolomitic sovite	Calcite, dolomite, apatite, magnetite, phlogopite, sulfides.	Fine to medium	Finely banded
	C_3	Sovite	Calcite, apatite, magnetite, phlogopite, dolomite, olivine, sulfides.	Medium to coarse	Non-carbonate minerals fewer than in other sovites. Banding less evident.
Northern Intrusions	C_4	Sovite	Calcite, apatite, magnetite, olivine, phlogopite, dolomite, sulfides.	Medium	
	C_5	Rauhaugite	Dolomite, apatite, phlogopite, magnetite, sulfides, calcite.	Medium to coarse	Very few silicates, oxides and sulfides
Dikes***	B_4	Beforsite	Dolomite, phlogopite, magnetite, calcite	Fine	Intruded in the C_4 sovite
	B_5	Beforsite	Dolomite, calcite, apatite, magnetite, phlogopite, sulfides.	Medium to fine	Offshoot of the C_5 rauhaugite in the C_4 sovite
Rocks from the contact between carbonatite intrusions C_2 and C_3	S	Sovite	Calcite, dolomite, apatite, phlogopite, magnetite, sulfides.	Medium to coarse	Diffuse banding
	B	Beforsite	Dolomite, calcite, apatite magnetite, sulfides	Medium	Diffuse banding
Reaction zone between the intrusions (C_1,C_3) and C_5) and the jacupirangite		Reaction rock	Phlogopite, alkali amphibole, calcite, magnetite, apatite, sulfides, ilmenite, clinohumite	Fine to coarse	Silicate rich bands alternate with carbonate rich bands (magnetite occurs in the silicate bands only
Host rock	JAC	Jacupirangite	Titanoaugite, titanomagnetite	Medium	

* *Other rock types cited in the text: alvikite (calcite, apatite, dolomite, phlogopite) and ijolite (clinopyroxene, nepheline).*

** *The minerals are cited in an estimated decreasing order of abundance*

*** *The characteristics cited for these two dikes refer specifically to them and not to the dikes in general that occur in the carbonatite bodies.*

developed varying in width from 10 cm to more than 2 m. Centimeter-wide bands of carbonate alternate with silicate-rich bands composed mainly of brown phlogopite, alkali amphibole, magnetite, and veins of carbonate a millimeter or so wide. The magnetites occur in the silicate-rich band only and contain platy exsolution lamellae of ilmenite.

The magnetites

As shown in Table 1, magnetite occurs in all five carbonatite intrusions. It is most abundant in C_1 and C_4, and least abundant in C_5. No evidence for oxidation of the magnetites was observed.

In carbonatite C_1, the magnetite crystals vary in size, but they are most commonly coarse grained. The largest magnetite crystals reach up to 4 cm in diameter. In the main concentrations of magnetite, associated with apatite and olivine, the crystals are octahedral, but more irregular crystals exhibiting the effects of resorption are widespread. Viewed in polished sections, the crystals are light purple and homogeneous. Inclusions of carbonates defined by sharp straight edges are found. Apatite inclusions are common.

C_2 carbonatite is equigranular, without local concentrations of magnetites or other minerals. The

magnetite diameters rarely exceed 2 or 3 mm, and the crystals tend to be rounded by resorption. Inclusions of carbonates similar to those found in the C_1 carbonatite are common.

The magnetite in C_3 carbonatite varies from a few millimeters up to 10 cm in diameter. In regions where the crystals are larger, the abundance is smaller. Crystals larger than 3 cm are twinned according to the spinel law. Inclusions of carbonates and more rarely sulfides occur within some magnetite crystals.

In C_4 carbonatite, magnetite may form large concentrations along with apatite, olivine, and phlogopite. The magnetite is anhedral to perfectly octahedral, with the octahedral forms occurring in the mineral concentrations. The magnetite varies in size from less than 1 mm to 1 cm. Inclusions of carbonates are present.

The magnetite in the C_5 carbonatite is an accessory mineral. It is light gray in polished sections, commonly anhedral, and always fine-grained, reaching diameters of 1 mm. No inclusions were observed.

The magnetites from all five carbonatite intrusions were analyzed with an electron microprobe. Analyses were also obtained for magnetites from the contact zone between C_2 and C_3, from the reaction zone between carbonatite and jacupirangite, and from intergrowths in sulfides.

Analytical procedure

Microprobe analyses were carried out using an ARL/EMX automated microprobe operated at 15 kV and 1.0 μA. Data were corrected by the computer program MAGIC IV. The accuracy of the analyses is $\pm 5\%$ of the amount present for concentrations up to 2 wt.% and $\pm 2\%$ of the amount present for major elements. The detection limit for minor elements calculated according to Reed (1973) is near 0.03 wt.%. Other details are given in the Appendix.

Magnetites from the carbonatite intrusions

The average analyses of the cores and rims of the zoned magnetites are listed in Table 2 and illustrated in a series of figures. Figures in the Appendix are identified with the prefix A. The results confirm the report of Boctor and Svisero (1978) that the minerals are composed essentially of the magnesioferrite–magnetite solid solution series, with striking zoning marked by increase of Fe_3O_4 from core to rim of minerals. The mineral compositions are conveniently represented in Figure 2. We compare mineral compositions by plotting weight fractions of components rather than cation fractions. Figure 2 is a modified combination of the two spinel prisms in general use, which each include an axis for chromites (Haggerty, 1976). Chromium is present only as a trace element in the Jacupiranga magnetites, and with removal of the chromite axis the remaining variables from the two spinel prisms are combined in Figure 2. The apex of the prism represents the magnesioferrite–magnetite series, and the base of the prism is defined by the spinel–hercynite series and the magnesian titanate–ulvöspinel series. The volume depicted in Figure 2 illustrates the fact that more than 95% of each analyzed spinel is represented by the magnesioferrite–magnetite series (see Table 2). The variations of Mg, Fe^{2+}, Fe^{3+}, Ti, and Al can be represented in projections from Figure 2. Table 2 gives values for other elements. MnO varies from 0.12% to 1.52%, and CaO from 0% to more than 0.6%. The elements Nb, Ta, and Zr were either not detectable, or rarely detectable but present in amounts below measurable limits. V occurs as a minor element, as also reported by Boctor and Svisero (1978).

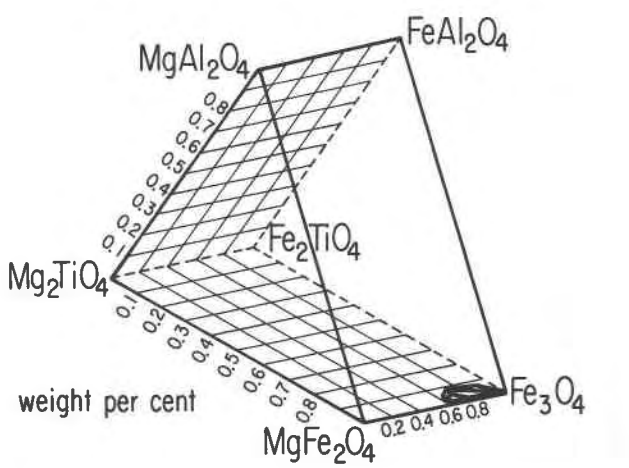

Fig. 2. Composition (wt.%) of magnetites from the carbonatite intrusions represented in a Cr-free spinel prism. The analyses in Table 2 occupy the outlined volume near Fe_3O_4.

Individual zoned crystals

Zoning is rather complex in most of the magnetites, with the complexity tending to increase with increasing grain size. The character of the zoning is illustrated in Figures A1 through A5 by the electron microprobe traverses across individual minerals

Table 2. Average compositions of magnetites from the carbonatite intrusions

	C_1											
	1		2		3		4		5		6	
	C(6)	R(6)	C(10)	R(9)	C(8)	R(6)	C(8)	R(8)	C(6)	R(6)	C(8)	R(7)
TiO_2	1.49	0.67	3.18	2.60	2.84	1.15	2.27	2.07	1.48	1.38	1.98	1.89
Al_2O_3	0.23	0.12	0.04	0.00	0.06	0.00	1.00	0.28	0.58	0.28	1.67	1.65
SiO_2	0.03	0.03	0.02	0.02	0.02	0.03	0.03	0.03	0.04	0.02	0.03	0.03
Fe_2O_3	66.4	67.7	65.2	65.8	65.6	68.6	66.9	67.7	68.6	68.7	67.6	67.3
FeO	30.5	30.1	27.0	27.3	26.4	26.4	23.5	24.5	22.0	22.2	21.3	20.9
MnO	0.20	0.12	0.81	0.68	0.73	0.48	0.76	0.72	0.71	0.80	0.69	0.76
CaO	0.05	0.37	0.01	0.16	0.01	0.24	0.02	0.30	0.03	0.47	0.00	0.20
MgO	1.14	0.61	4.08	3.46	4.24	3.26	5.98	4.97	6.30	5.63	7.45	7.29
TOTAL	100.04	99.72	100.34	100.02	99.90	100.16	100.46	100.57	99.74	99.48	100.72	100.02

	C_2											
	7		8		9		10		11		12	
	C(8)	R(8)	C(10)	R(10)	C(6)	R(6)	C(11)	R(8)	C(7)	R(7)	C(9)	R(6)
TiO_2	0.35	0.30	0.97	0.94	0.71	0.68	1.00	1.10	0.90	0.69	0.50	0.45
Al_2O_3	0.59	0.64	1.37	0.97	1.52	0.91	1.19	0.91	2.69	1.24	1.93	1.28
SiO_2	0.02	0.01	0.04	0.03	0.02	0.03	0.02	0.02	0.04	0.03	0.02	0.03
Fe_2O_3	70.2	69.3	69.3	69.3	69.8	69.8	70.8	70.5	71.3	70.1	71.1	71.3
FeO	24.6	26.2	21.3	22.1	19.9	20.6	17.5	17.4	15.5	18.0	15.3	15.5
MnO	0.69	0.52	1.03	1.18	1.04	1.19	1.36	1.52	0.96	1.30	1.16	1.45
CaO	0.07	0.33	0.07	0.47	0.03	0.50	0.03	0.43	0.03	0.41	0.08	0.47
MgO	4.09	2.87	6.47	5.48	7.24	6.13	8.83	8.40	9.94	7.79	9.95	9.19
TOTAL	100.61	100.17	100.55	100.47	100.26	99.84	100.73	100.28	101.36	99.56	100.04	99.67

	C_3											
	13		14		15		16		17		18	
	C(14)	R(12)	C(10)	R(9)	C(4)	R(4)	C(12)	R(9)	C(11)	R(10)	C(6)	R(6)
TiO_2	1.54	0.85	1.47	1.37	0.57	0.33	0.43	0.33	0.64	0.49	0.60	0.55
Al_2O_3	1.14	0.13	1.55	0.34	0.89	0.11	2.40	1.51	2.16	0.39	2.11	0.81
SiO_2	0.03	0.03	0.02	0.03	0.01	0.03	0.02	0.02	0.02	0.03	0.01	0.03
Fe_2O_3	68.5	70.1	68.0	68.6	71.7	70.5	70.5	70.8	70.3	71.3	70.4	69.7
FeO	22.2	23.7	20.7	22.5	18.4	24.6	17.3	18.9	17.1	19.6	16.7	21.4
MnO	0.98	0.85	0.99	1.10	0.71	0.61	0.85	1.25	0.78	1.04	1.03	1.03
CaO	0.03	0.61	0.02	0.43	0.01	0.30	0.01	0.38	0.01	0.30	0.01	0.36
MgO	6.32	4.45	7.10	5.30	8.35	3.82	9.03	7.27	9.26	6.90	9.29	5.69
TOTAL	100.74	100.72	99.85	99.67	100.64	100.30	100.54	100.46	100.27	100.05	100.15	99.57

	C_4						C_5					
	19		20		21		22		23		24	
	C(10)	R(8)	C(10)	R(10)	C(13)	R(9)	C(9)	R(9)	C(12)	R(11)	C(14)	R(10)
TiO_2	0.21	0.20	0.23	0.25	0.30	0.14	0.42	0.26	0.22	0.21	0.27	0.23
Al_2O_3	0.04	0.01	1.42	0.40	1.06	0.26	0.02	0.03	0.32	0.13	0.86	0.16
SiO_2	0.02	0.02	0.02	0.03	0.02	0.02	0.03	0.02	0.02	0.03	0.05	0.03
Fe_2O_3	69.4	69.4	69.6	69.7	70.4	70.9	69.1	69.3	69.2	69.0	69.1	69.6
FeO	27.6	27.6	22.4	24.1	21.9	23.5	28.8	29.3	28.7	29.5	28.6	29.6
MnO	0.34	0.34	0.71	0.71	0.63	0.57	0.17	0.12	0.26	0.22	0.32	0.22
CaO	0.16	0.46	0.02	0.42	0.01	0.32	0.27	0.50	0.03	0.26	0.04	0.34
MgO	1.90	1.71	5.52	3.84	5.90	4.44	1.43	0.91	1.56	0.89	1.83	0.93
TOTAL	99.67	99.74	99.92	99.45	100.22	100.15	100.24	100.44	100.31	100.24	101.07	101.11

1-Sovite 5-Sovite 9-Rauhaugite 13-Sovite 17-Sovite 21-Sovite
2-Sovite 6-Sovite 10-Sovite 14-Sovite 18-Rauhaugite 22-Rauhaugite
3-Sovite 7-Rauhaugite 11-Sovite 15-Sovite 19-Sovite 23-Rauhaugite
4-Sovite 8-Sovite 12-Sovite 16-Sovite 20-Beforsite 24-Beforsite

C = core of mineral R = rim of mineral (X) = number of measurements

from each of the five carbonatite intrusions. Descriptions of the figures are given in the Appendix.

The zoning trends from cores to rims represented in terms of oxides are as follows: (1) MgO decreases, (2) Fe_2O_3 and CaO increase, (3) TiO_2 decreases or remains constant, (4) Al_2O_3 decreases except for C_1 where it remains constant, (5) FeO increases except for C_1 where it decreases, and (6) MnO remains constant, or exhibits a slight decrease (C_1) or slight increase (C_3).

Examinations of these zoning profiles leads to the following conclusions about variations in solid solutions from core to rim: (1) Fe_3O_4 increases, (2) $MgFe_2O_4$ decreases, (3) in magnetites from C_1, Fe_2TiO_4 decreases with insignificant variation of $MgAl_2O_4$, (4) in magnetites from C_2 to C_5, $MgAl_2O_4$ decreases with only slight variation of Fe_2TiO_4, (5) $MnFe_2O_4$ (jacobsite produced by replacement of FeO or occasionally MgO by MnO) generally decreases, but it increases in some samples, (6) $CaFe_2O_4$ (produced by replacement of MgO in magnesioferrite by CaO) increases.

It is evident that ulvöspinel plays an important role in the zoning of magnetite of the C_1 carbonatite, but it is not important for magnetites from the other carbonatites. The magnetites in the C_1 carbonatite also differ from those in the other carbonatites because $MgAl_2O_4$ remains nearly constant, whereas it decreases from core to rim in magnetites from the other carbonatites.

Core compositions and ranges of zoning

Because the compositions of the cores of the magnetites should reflect the early history of their crystallization in each carbonatite intrusion, these compositions are reviewed and compared first. The zoning trends will be analyzed subsequently, using the chemical variation trends of the core compositions in each of the five carbonatite intrusions as a basis for comparison. The average core compositions from Table 2 can be related to their positions within the spinel prism of Figure 2 in the projections illustrated in Figures 3, 4, and 5.

The variation of FeO/(FeO+MgO), corresponding to the main trend along the magnesioferrite to magnetite edge of the spinel prism, is shown for the core compositions of magnetites in each of the five intrusions in Figure 3. The values are arranged in order of decreasing age of the intrusions, from C_1 to C_5. The core compositions from each intrusion occupy a fairly wide range, except for C_5. The ranges for C_3, C_4, and C_5 barely overlap; that for C_2 overlaps C_1, C_3, and C_4; and that for C_1 overlaps the other four intrusions. With the exception of the magnetites for C_1, the highest value of FeO/(FeO+MgO) for the cores of magnetites in each intrusion decreases with decreasing age.

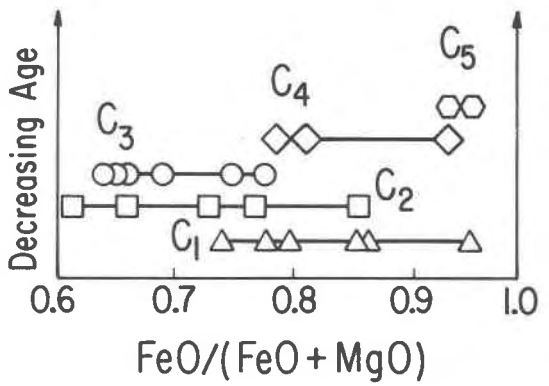

Fig. 3. Range of FeO/(FeO+MgO) of the core compositions (Table 2) for the five carbonatite intrusions according to decreasing age (Fig. 1, Table 1). C_1—triangles, C_2—squares, C_3—circles, C_4—diamonds, and C_5—hexagons.

Figures 4A, 5, and A6 show the same analyses in projections from the spinel prism of Figure 2. The projections correspond in terms of geometry to the standard projections of Irvine (1965), but compositions are in weight fractions rather than in cation fractions. Two additional points are given, B_4 and B_5 representing the core compositions of magnetites from two beforsite dikes associated with carbonatites C_4 and C_5, respectively (see Table 1). Figure 6 compares the Mn content with Mg content of the

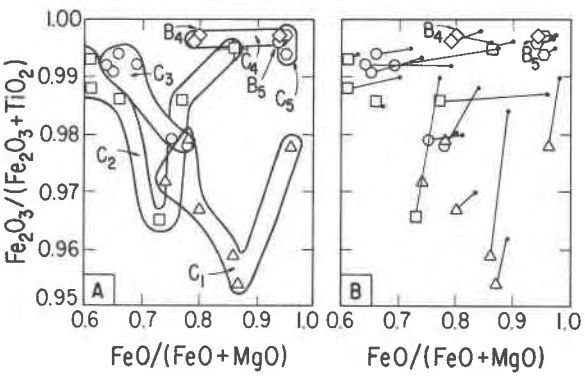

Fig. 4. Average core and rim compositions of magnetites (Table 2) in projections from the spinel prism (Fig. 2). A representative range of values is shown for one of the average points. A. Core compositions. See Figure 3 for symbols. B. The core compositions connected by lines to corresponding rim compositions (dots) showing zoning trends.

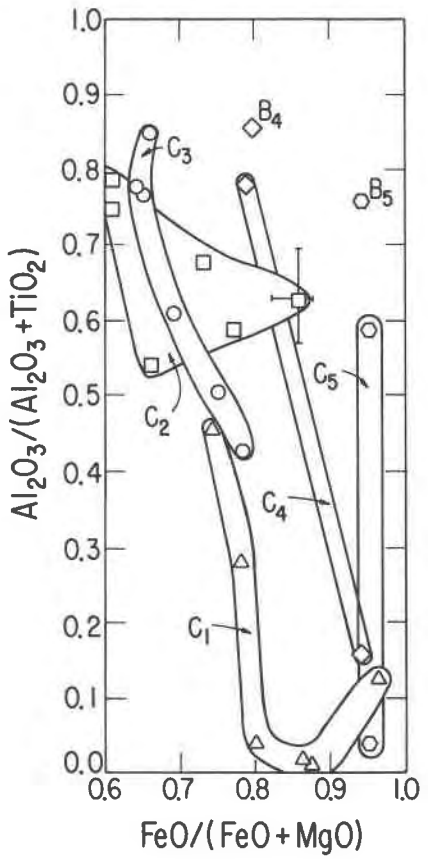

Fig. 5. Average core compositions of magnetites projected from the spinel prism (Figure 2). See legend for Figure 4.

core magnetites. Descriptions of these figures are given in the Appendix.

Figures 3, 4, 5 and 6 show that the cores of the magnetites from each of the five carbonatite intrusions are chemically distinct and distinguishable. Overlaps in composition in some diagrams are not present in other diagrams. The carbonatite intrusions C_2 and C_3 include dolomitic rocks among the sovites, but both rock types have similar magnetites.

The zoning ranges from core to rim of each magnetite analyzed are shown by the connecting lines in Figures 4B, A6B, A7 and A8. Most of these lines probably have superimposed on them variations of the kind illustrated in the detailed compositional profiles of Figures A1 through A5. All zoning has a component in the direction of increasing FeO/(FeO+MgO), equivalent to a decreasing number of Mg cations in Figure A8. In Figure 4B, most lines are directed towards the upper right hand corner representing the Fe_3O_4 end-member. For the magnetite core compositions (Fig. 4A) this same trend appears to be superimposed on a dominant trend in C_1, C_2 and C_3 directed towards the lower right corner, which corresponds to enrichment in ulvöspinel (see Fig. 5). Additional details are given in the Appendix.

The chemical variation trends exhibited by the magnetite core compositions are well illustrated in the projections from the spinel prism in weight per cent, but the zoning exhibited by individual magnetites within the intrusions is better represented and interpreted in terms of element substitutions.

Element substitutions

The analyses in Table 2 were recalculated in terms of cation numbers. Element substitutions for Fe^{3+} are illustrated in Figure 7. Substitution by Al^{3+} is represented by the replacement line for the ratio 1:1, and substitution by Ti+Si according to $2Fe^{3+} = Ti^{4+} + Fe^{2+}$, as in the magnetite–ulvöspinel series, is represented by the replacement line for the ratio 2:1. Stoichiometric magnetites plot between these two lines. The substitution of Al_2O_3 is more important for the core magnetites in intrusions C_2 to C_5. The magnetites from C_1 plot closer to the 1:1 replacement line, confirming their greater content of ulvöspinel. All zoning trends are directed towards maximum site occupancy by Fe^{3+} as shown in Figure 7B. This trend, coupled with the trend of increasing FeO (Figure 4B), demonstrates the tendency of magnetites to zone towards Fe_3O_4. The Appendix includes additional comments on element substitutions and zoning trends.

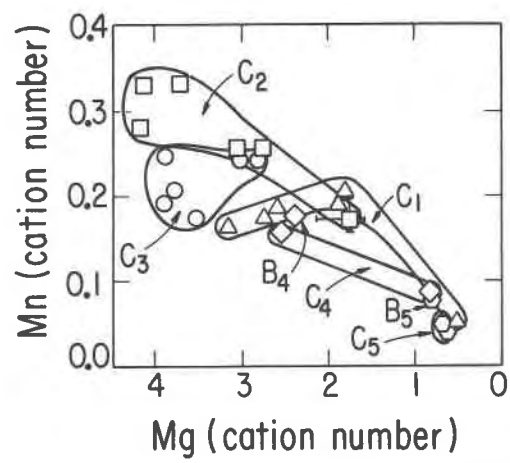

Fig. 6. Magnetite analyses for Mn and Mg (Table 2). See legend for Figure 4. A representative range is shown for one average point.

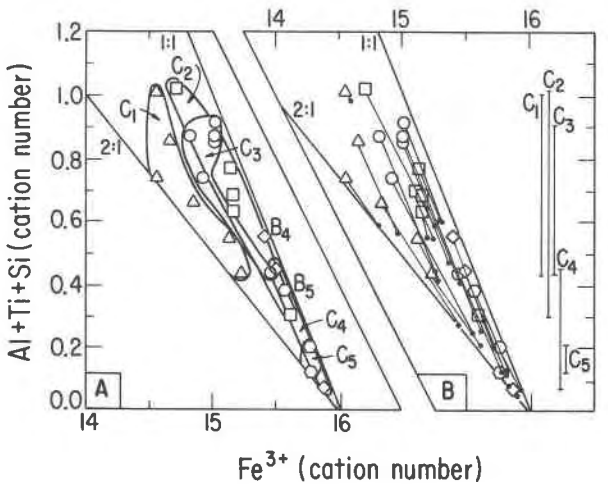

Fig. 7. Magnetite analyses (Table 2) recalculated in terms of cations. A. Core compositions. See Figure 3 for symbols. B. Core (symbols) and rim (dots) composition. See text for interpretation. The range of Al+Ti+Si for magnetite cores from each intrusion is shown on the right of B.

The range of Al+Ti+Si for the magnetite cores is shown for each intrusion in Figure 7B. The highest values for each intrusion decrease with decreasing age from C_2 to C_5, and the highest value for C_1 is barely distinguishable from that for C_2. This shows the same tendency of increasing Fe^{+3} in the sequence C_2 to C_5 as that shown by the individual zoning trends. A similar pattern was observed for the highest FeO/(FeO+MgO) in the core magnetites (Fig. 3).

Magnetites from special locations

The ranges of compositions of the magnetites in the main bodies of the five carbonatite intrusions provide a framework for comparison of the compositions of magnetites from several other, more specialized environments in the Jacupiranga Complex. The average analyses of magnetites from four different environments are listed in Table 3, and in Figure 8. The field relationships of the rocks listed were outlined briefly in connection with the geology, and Table 1.

The contact between carbonatite intrusions C_2 and C_3

In an attempt to find evidence to account for the diffuse banding and the increase in dolomite at the intrusive contact between carbonatites C_2 and C_3 (Fig. 1), magnetites from the calcitic (S) and colomitic rocks (B) were analyzed and plotted in Figures 8 and 9, which show the composition ranges of magnetite cores from the five intrusions, transferred from Figures 4A, A6, and 6.

The core composition of the magnetite from the dolomite rock in the contact zone (B) does not correspond precisely to any of the ranges of composition characterized for the five carbonatites. In Figure 8B, it plots above the intrusive rocks, very close to the position of the beforsite dike (B_5 in Figure A6), which is an offshoot of the carbonatite intrusion C_5. Thus, it has chemical characteristics more similar to magnetite in the beforsite dikes than to any other magnetites.

The core composition of the magnetite from the calcite rock in the contact zone (S) plots within the areas for intrusion C_1 in Figures 8A and 9, within the area for C_3 if plotted in Figure 5, and separately from all intrusive rocks in Figure 8B.

A microprobe profile across one of the magne-

Table 3. Average compositions of magnetites from special locations

	1		2		3		4	5
	C(8)	R(6)	C(5)	R(3)	C(2)	R(2)	(2)	(1)
TiO_2	2.09	1.81	0.79	0.74	11.3	9.88	11.0	7.28
Al_2O_3	1.83	0.91	1.11	0.53	3.07	2.26	2.48	1.91
SiO_2	0.04	0.03	0.05	0.01	0.09	0.05	0.03	0.00
Fe_2O_3	66.1	66.5	66.4	66.7	46.1	49.2	47.2	55.1
FeO	23.0	23.5	28.3	29.1	33.3	32.5	33.2	32.8
MnO	0.80	0.91	0.31	0.21	0.60	0.60	0.51	0.18
CaO	0.02	0.30	0.07	0.37	0.02	0.11	0.11	0.00
MgO	6.20	5.07	1.93	1.07	5.24	4.67	4.99	3.52
TOTAL	100.08	99.03	98.96	98.73	99.72	99.27	99.52	100.79

	6	7	8	9	10	11	12	13
	(7)	(16)	(8)	(10)	(9)	(2)	(2)	(2)
TiO_2	1.00	0.90	2.56	1.52	1.47	0.02	0.00	0.05
Al_2O_3	0.00	0.00	0.20	0.43	0.00	0.03	0.00	0.00
SiO_2	0.04	0.04	0.04	0.08	0.03	0.06	0.11	0.05
Fe_2O_3	67.0	67.8	66.7	66.6	66.3	68.2	68.8	68.2
FeO	31.5	31.2	24.8	29.7	30.4	28.8	26.9	28.5
MnO	0.05	0.07	0.86	0.32	0.19	0.30	2.97	0.21
CaO	0.14	0.04	0.02	0.01	0.01	0.04	0.13	0.39
MgO	0.14	0.44	5.09	1.69	1.07	0.94	0.56	0.93
TOTAL	99.87	100.49	100.24	100.35	99.47	98.39	99.47	98.33

1 -- Sovite in the contact of C_2 and C_3.

2 -- Beforsite in the contact of C_2 and C_3.

3,4 -- Jacupiranguite. No ilmenite lamellae detected.

5 -- Jacupiranguite. The nearest measurement to an ilmenite lamella in an exsolved grain

6,7 -- Exsolved magnetite in the reaction rock of the C_1 intrusion.

8 -- Exsolved magnetite in the reaction rock of the C_3 intrusion.

9,10 -- Exsolved magnetite in the reaction rock of the C_5 intrusion.

11 -- Magnetite intergrowth with pyrite in a rauhaugite from the C_3 intrusion.

12 -- Magnetite intergrowth with pyrite in a sovite from the C_3 intrusion.

13 -- Magnetite intergrowth with pyrite in a sovite from the C_4 intrusion.

C = core of mineral R = rim of mineral (X) = number of measurements

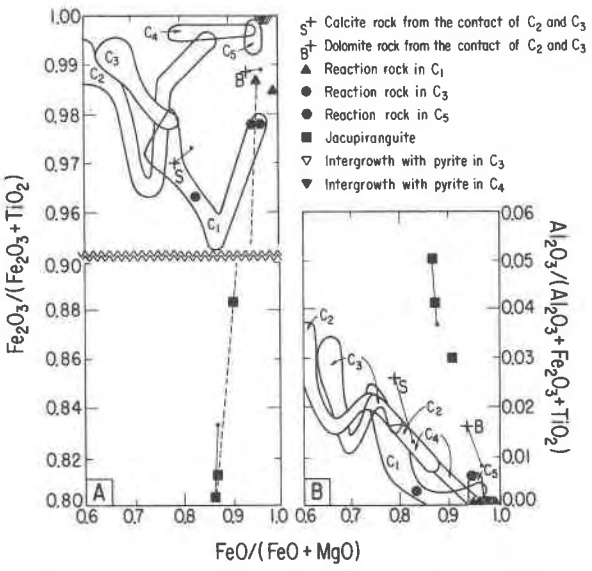

Fig. 8. Magnetites from special locations (Table 3) compared with the ranges of average core compositions for each of the five carbonatite intrusions outlined in Figures 4A and A6A. Dots are rim compositions.

tites showed some variation in TiO_2, and a significant decrease in Al_2O_3 from core to rim, similar to the variations in magnetite from C_3. The strong zoning for Al_2O_3 indicates that the calcite rock in the contact zone is not related to C_1, despite its coincidence with the areas for C_1 in some figures. This is consistent with the fact that C_1 is older than C_2 and C_3, according to the field relations.

Magnetites from the reaction between carbonatite and jacupirangite

Magnetite compositions from the banded reaction rocks (silicate bands) associated with carbonatite intrusions C_1, C_3, and C_5 are presented in Table 3, along with magnetite from jacupirangite, and these are compared with magnetite from the carbonatites in Figures 8 and 9. The magnetites from jacupirangite have compositions quite distinct from those in the carbonatite intrusions. The magnetites in the reaction bands are similar in composition to those in the carbonatites, with somewhat higher TiO_2.

The jacupirangites contain titanomagnetite which exhibit some exsolution of ilmenite within a centimeter or two from the banded reaction rock. Analyses 3 and 4 in Table 3 are from a jacupirangite titanomagnetite with no detectable ilmenite lamellae, and analysis 5, with less TiO_2, is for magnetite adjacent an ilmenite lamella in an exsolved mineral. The magnetites from the carbonatites (Table 2) are too low in titanium to yield the exsolved magnetites of the reaction rock (Table 3). Therefore, the exsolved magnetites in the reaction bands are probably derived from titanomagnetites in the jacupirangite. However, as discussed in the Appendix, the chemical relationships cannot be explained in terms of exsolution alone.

Magnetite intergrowth with pyrite

Patches and strings of magnetite in euhedral and subhedral crystals of pyrite occur commonly in carbonatites C_3 and C_4, less often in C_1 and C_2, and not in C_5. The magnetites are light grey in reflected light. Three analyses from examples in C_3 and C_4 are presented in Table 3, and compared with the other magnetites in Figures 8 and 9. They are extremely low in TiO_2 and Al_2O_3, very low in MgO, and very rich in Fe_3O_4. The relationship between Mn and Mg in these magnetites contrasts sharply with that in the discrete magnetite crystals, as shown in Figure 9. The number of Mg cations in the intergrowth magnetites is at the extreme low end of the range for the discrete magnetites, and the range of Mn cations extends to much higher levels. The intergrowth magnetites plot on lines transverse to the variation in the discrete carbonatite magnetites, with the 1:1 slope representing the substitution of Mg by Mn.

Inclusions in magnetite crystals

The magnetites from the carbonatites contain many inclusions, commonly composed of more than one mineral, making it difficult to analyze them with the electron microprobe. However, the analy-

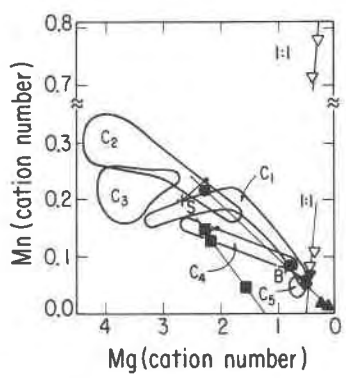

Fig. 9. Magnetites from special locations (Table 3) compared with the ranges of average core compositions for each of the five carbonatite intrusions outlined in Figure 6. For symbols see Figure 8. Dots are rim compositions.

ses were sufficient to determine the major minerals present. Inclusions of carbonate, apatite, phlogopite, and spinel are most abundant. The carbonates, with sharp straight edges, are dolomite or calcite, and rarely siderite or magnesite. Spinel ($MgAl_2O_4$) inclusions occur either alone or with carbonates. Hercynite was identified in one inclusion. High values of SiO_2 recorded in some analyses of spinel ($MgAl_2O_4$) indicate the coexistence of a silicate phase. One analysis of a spinel inclusion was reported by Mitchell (1978). Rare inclusions of ilmenite were found in some C_1 and C_3 magnetites.

Comparison with previous results from the Jacupiranga carbonatite

Figure 10 reproduces from Figures 4A and A6 the ranges of average compositions for the cores of the magnetites from the five carbonatite intrusions at Jacupiranga. The magnetite analyses presented by Mitchell (1978) and Boctor and Svisero (1978) for the Jacupiranga carbonatite are plotted for comparison. They reported no zoning. Their analyses are generally similar to our results, despite the fact that their samples were obtained from a higher level in the quarry some years before the collection of our rocks. The three analyses of magnetites given by Mitchell (1978) contain exsolved ilmenite lamellae. More details are given in the Appendix. Melcher (1966) presented an analysis of a magnetite concentrate from the Jacupiranga carbonatite, which is similar to those from the C_1 carbonatite (Table 2).

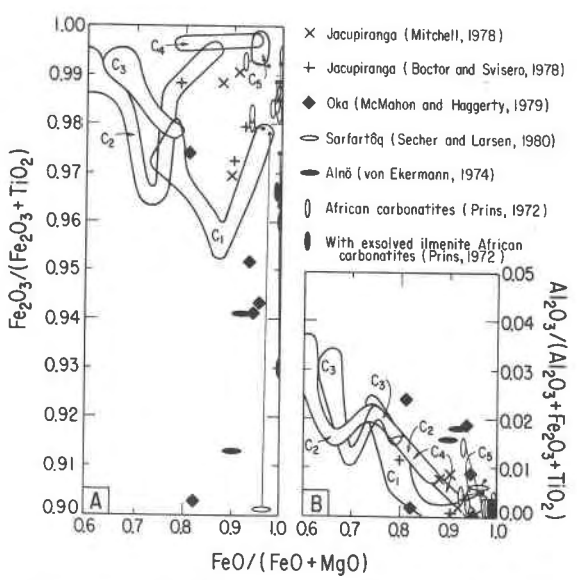

Fig. 10. Jacupiranga magnetite analysis by Mitchell (1978) and Boctor and Svisero (1978), and from other carbonatites, compared with the ranges of average core compositions for each of the five Jacupiranga carbonatite intrusions outlined in Figures 4A and A6A. Dots are rim compositions.

Comparison with magnetites from other carbonatites

Mitchell (1978) and Boctor and Svisero (1978) compared their analyses of magnetites from Jacupiranga with a selection of the few analyses published for magnetites from other carbonatites. Some of these analyses, and others, are compared in Figure 10 with the ranges of core compositions of magnetites from the five Jacupiranga carbonatite intrusions. The magnetites from other carbonatites are even more closely crowded into the Fe_3O_4 corner of the spinel prism than those from Jacupiranga (Fig. 2), but many of the others contain more Ti. A detailed review of Figure 10, together with data on MnO, is presented in the Appendix.

Magnetite compositions and magmatic evolution

The magnetites from the five carbonatite intrusions of Jacupiranga, and from carbonatites in general, occupy a very restricted range of compositions, as shown in Figure 2 and by Mitchell (1979). However, the fact that the magnetite core compositions in each of the five intrusions are chemically distinguishable from each other indicates that they are sensitive to conditions of formation, and they should therefore provide useful petrogenetic information.

The origin of carbonatites

Theories for the origin of carbonatites have been reviewed in detail by Heinrich (1966, chapter 10), Tuttle and Gittins (1966), Carmichael *et al.* (1974, chapter 10), Le Bas (1977, chapters 23 and 24), and Gittins (1978). There was general reluctance to accept early proposals that carbonatites were magmatic, partly because the fusion temperature of calcite, above 1300°C, was much higher than estimated emplacement temperatures of carbonatites (700°C to 350°C). There was much debate about the relative merit of hypotheses involving intrusive marbles, xenolithic marbles, hydrothermal or carbothermal deposits, and metasomatic replacement of various alkalic rocks. Experimental evidence that calcite could be precipitated from melts at moderate temperatures and pressures in the system $CaO–CO_2–H_2O$ (Wyllie and Tuttle, 1960) led to general acceptance of a magmatic origin for most carbonatites, with processes involving crystalliza-

tion differentiation or liquation of a carbonated nephelinitic magma. There is experimental evidence for both processes (Koster van Groos and Wyllie, 1966, 1973; Wyllie, 1978). The prospect that carbonatitic melts could be present in the upper mantle (Wyllie and Huang, 1975) does not justify suggestions that near-surface carbonatites were precipitated from primary, mantle-derived carbonatite magmas. Mitchell (1979) presented arguments opposing such suggestions.

The chemical variation of the magnetites in the Jacupiranga carbonatites is so systematic that it would be difficult to account for it by any process other than magmatic. The challenge is to explain the mineralogy of the five carbonatite intrusions in terms of successive intrusions derived from a single evolving parent nephelinitic magma, or from successive batches of silicate magma. The major processes to evaluate are (1) fractional crystallization of parent silicate melt(s), (2) separation of immiscible liquid fractions from silicate melt(s), and (3) fractional crystallization of a parent carbonatite magma derived previously from a silicate magma.

FeO/(FeO+MgO) and its time significance

It is expected that FeO/(FeO+MgO) for minerals crystallizing from a magma will increase with progressive crystallization, that is, with decreasing temperature and increasing time. Every magnetite analyzed in the carbonatite intrusions of Jacupiranga exhibits a component of zoning with increasing FeO/(FeO+MgO), which is consistent with this expectation (Figs. 4B, A6B, and A7). Therefore, we will assume that FeO/(FeO+MgO) for magnetite in a given intrusion correlates with a particular temperature and time in its history.

The cores of magnetites in the four intrusions C_1 to C_4 (Fig. 3) display a wider range of FeO/(FeO+MgO) than the ranges of magnetite compositions from other carbonatites illustrated in Figure 10. The measured compositions at the centers of random slices through zoned magnetites would be higher than the actual core compositions, but comparison of the zoning in Figures 4B, A6B and A7 with the ranges of core compositions in Figures 4A, A6A and 5 demonstrates that this effect is insufficient to explain the complete ranges of measured core compositions. Thus, it is evident that the magnetite crystals did not nucleate together at the beginning of crystallization of each carbonatite intrusion. Most likely, additional magnetite crystals nucleated through the crystallization intervals, but there is a possibility that influxes of more evolved carbonatite magma brought in magnetites with higher FeO/(FeO+MgO).

Within a particular carbonatite intrusion, assuming that crystallization of the magnetite began within the carbonatite magma and not in the parent magma from which the carbonatite was derived, the lowest value of FeO/(FeO+MgO) in a magnetite core should represent the earliest time in the history of that carbonatite intrusion. There is an excellent correlation in Figure 3 between the lowest value of this ratio for each intrusion and the age of the intrusion determined from field relationships, except for C_1.

The ranges of composition of the magnetite cores in C_3, C_4 and C_5 succeed each other closely, with only very slight overlap (Fig. 3), which is consistent with a conclusion that these three carbonatites represent a continuum in time and chemical evolution of carbonatite magma. From this evidence, the three intrusions could represent successive batches of magma from a single evolving body of magma, or the magma that produced intrusion C_3 could have differentiated further to produce carbonatites C_4 and C_5 in succession.

The range of core compositions for the magnetites from C_2 begins with FeO/(FeO+MgO) lower than that of C_3, consistent with the age relationships (Fig. 3), but the range of core compositions continues further than, and thus later than, the range for C_3 and into the center of the range for C_4. This suggests that the chemical evolution of C_2 overlaps the history of C_3 and C_4, which is not inconsistent with the possibility that C_3, or the sequence C_3–C_4–C_5, was derived by differentiation of and physical separation from the parent magma which produced carbonatite C_2.

The lowest value of FeO/(FeO+MgO) for magnetite cores in C_1 is higher than values in C_2 and C_3. The simple interpretation that C_1 is younger than C_2 and C_3 is inconsistent with the field relationships (Figs. 1 and 3). The range of core compositions for C_1 extends to the highest values recorded in the youngest intrusion, C_5.

The parent from which C_1 was derived, be it carbonatite or silicate magma, may have reached a stage in chemical evolution different from that of the parent(s) from which C_2 through C_5 were derived. There appears to be some kind of interruption in magmatic evolution between the crystallization of magmas producing C_1, C_2, and C_3–C_4–C_5, with the more marked hiatus between C_1 and C_2.

These prospects can be explored in more detail when data from coexisting minerals become available.

Core composition trends and zoning trends

If the successive values of FeO/(FeO+MgO) in the ranges of magnetite core compositions reflect the successive nucleation of magnetite crystals with decreasing temperature and increasing FeO/(FeO+MgO) of the magmas, the simplest interpretation, then the zoning ranges of individual crystals should follow the same trends as the core compositions. This is broadly true for the variation of $Al_2O_3/(Al_2O_3+Fe_2O_3+TiO_2)$ in Figure A6, and broadly true (with a few notable exceptions discussed below) for the variation of $Al_2O_3/(Al_2O_3+TiO_2)$ in Figure 5 and A7. The variation of $Fe_2O_3/(Fe_2O_3+TiO_2)$, however, differs markedly from the simple pattern, and confirms the distinctive chemical character of the magnetites in C_1 compared with those in the other four intrusions (Figs. 4A and B).

The core compositions of magnetites from carbonatites C_2 to C_5 have values of $Fe_2O_3/(Fe_2O_3+TiO_2)$ greater than 0.978, with one exception from C_2 with a low value near 0.965 (Fig. 4A). Their zoning lines are directed almost horizontally, indicating little variation in Fe_2O_3/TiO_2 during crystallization of the magmas. The same trend is broadly defined by the core compositions of the magnetites in these four intrusions, except for the two latest magnetites from C_3 which drop down to values just below 9.8, and for the exception from C_2 noted above.

The core compositions of all magnetites from C_1 have $Fe_2O_3/(Fe_2O_3+TiO_2)$ less than 0.98. The four C_1 core compositions lowest in Figures 4A and B illustrate a trend of $Fe_2O_3/(Fe_2O_3+TiO_2)$ decreasing from 0.97 to 0.95 with increasing FeO/(FeO+MgO). (The two lowest points for core magnetites from C_3 indicate a parallel trend for C_3, but the zoning trends in the two intrusions are quite different). The zoning of individual magnetites in C_1 is directed approximately perpendicular to the core trend defined by the four magnetites, that is, with increasing $Fe_2O_3/(Fe_2O_3+TiO_2)$ for increasing FeO/(FeO+MgO). The two magnetite cores in C_1 with values of $Fe_2O_3/(Fe_2O_3+TiO_2)$ near 0.98, higher than the four defining a core trend from 0.97 to 0.95, are displaced from the core trend in the direction of the zoning paths, and their zoning lines continue in the same direction.

There must be at least two effects associated with the nucleation and crystallization of the magnetites in carbonatite C_1. The zoning represents the changing chemistry of the carbonatite magma during crystallization and, therefore, the opposing trend with respect to $Fe_2O_3/(Fe_2O_3+TiO_2)$ illustrated by the set of four magnetite cores must be caused by some other effect, presumably related in some way to the parent magma(s) from which the carbonatite magma was derived, either a carbonatite predecessor, or silicate parent.

The magnetites of intrusion C_1 are also distinguished from those of the other intrusions by their core compositions (Figures 4A and 5) and zoning trends (Fig. 4B). Their distinctive chemistry compared with the magnetites in the other four intrusions was also noted in the illustration of their zoning with respect to Fe_2TiO_4 and $MgAl_2O_4$ (Figs. Al through A5), and the element substitutions (Fig. 7).

The zoning of magnetites from intrusion C_1 illustrated in Figure 4B is towards the higher level of $Fe_2O_3/(Fe_2O_3+TiO_2)$ characteristic of magnetites from the other four intrusions, indicating that the core magnetite cores in C_1 crystallized from a magma less evolved than those which yielded intrusions C_2 through C_4. The less evolved magma was probably formed earlier in the history of the complex than the other magmas, which is consistent with the age relationships based on field relationships. The inconsistency for C_1 in Figure 3, considering the lowest value of FeO/(FeO+MgO) as indicator of relative ages of intrusions, remains unexplained.

There is one anomaly in Figure 4. The magnetite from C_2 with low $Fe_2O_3/(Fe_2O_3+TiO_2)$ has core composition and zoning trend corresponding to those of magnetites in C_1. In other respects, this particular magnetite does not differ significantly from the others in C_2 (Figs. 4 and 5).

Apart from the contrast between magnetites from C_1 compared with those from the other intrusions in Figure 4B, the zoning trends exhibit agreement with the general trends of core compositions, but there are a few examples of zoning reversals. The last C_2 magnetite in Figure A6B reverses, exhibiting an increase of $Al_2O_3/(Al_2O_3+Fe_2O_3+TiO_2)$ from core to rim, and it shows the equivalent reversal in Figure A7. Three other exceptions in Figure A7 (two from C_1 and one from C_5) illustrate a reversal of the zoning trend, with increase of $Al_2O_3/(Al_2O_3+TiO_2)$ from core to rim.

Figure 6 illustrates a general variation in magne-

tite cores of decreasing Mn with decreasing Mg, which corresponds to increasing FeO/(FeO+MgO) and progressive crystallization. The Mn content may increase or decrease from core to rim of individual crystals, with much more variability than zoning for the other elements (Figs. 4B, A6B, and A7). There is a tendency for magnetites with high Mg to zone towards increasing Mn, and for those with lower Mg to zone towards decreasing Mn, but there are some exceptions among magnetites richer in Mg (Figure A8). Note that the magnetites from C_1 fit the general pattern, but the earliest magnetites do not contain as much Mn as most of the magnetites in C_2, and as half of those in C_3. Given the field (Fig. 1) and chemical (Fig. 4B) evidence that C_1 is older and less chemically evolved than the other four carbonatite intrusions, the relatively low Mn content of its more Mg-rich magnetites is consistent with the previous conclusion that there is some kind of chemical hiatus between C_1 and C_2–C_5, probably related to their respective parent magmas.

Beforsite dikes

In Figures 4A and B, the magnetite core compositions and zoning in the dike rocks B_4 and B_5 are indistinguishable from those in the associated intrusions, C_4 and C_5. In Figures A6 and 5, however, the magnetite cores in the dikes are relatively higher in $Al_2O_3/(Al_2O_3+Fe_2O_3+TiO_2)$ and $Al_2O_3/(Al_2O_3+TiO_2)$ compared with the magnetite cores in C_4 and C_5, for comparable values of FeO/(FeO+MgO). This indicates that the dikes crystallized from magmas representing earlier stages of evolution than the magmas precipitating the carbonatite bodies which they cut (C_4) or are derived from (B_5 is an offshoot from C_5, Table 1).

The dike B_4 cannot represent a differentiate from the intrusion C_4 which it cuts, and its occurrence suggests the persistence below the intrusion C_4 of a magma body at a somewhat earlier stage of chemical evolution than C_4. Similarly, the dike B_5 emanating from C_5 cannot represent a differentiate from the intrusion C_5. It could represent the initial intrusion of carbonatite C_5, which was followed by the magma body producing the somewhat more evolved carbonatite C_5.

Contact region between intrusions C_2 and C_3

The magnetite data for the calcite- (S) and dolomite-rocks (B) in the contact zone with diffuse banding between intrusions C_2 and C_3 was reviewed in connection with Figures 8 and 9. The simplest interpretation of the data so far available is that the calcite rock in the contact zone could be related to either intrusion, C_2 or C_3, but is probably related to C_3. The formation of the dolomite-rock in this zone appears to be most closely related (in terms of magnetite chemistry) to the beforsite dikes (B_5) emanating from the youngest intrusion, C_5. We concluded that the dikes B_5 could have been the precursors of the magma forming intrusion C_5, and perhaps this material also penetrated the carbonatite complex along the earlier contact between C_2 and C_3. Alternative explanations involve metasomatism by the introduction of fluids from uncertain sources. More information is required for a satisfactory interpretation.

Reaction zone between carbonatite and jacupirangite

The data for magnetite present in jacupirangite and in the banded rocks developed between carbonatite and jacupirangite were reviewed in connection with Figures 8 and 9. The jacupirangite contains titanomagnetite which exsolved ilmenite in the reaction bands. The magnetites in the silicate layers (magnetite is absent from the carbonatite layers) are similar in composition to some of those in the associated carbonatite intrusions, but with somewhat higher TiO_2. They originally contained much more TiO_2 than the magnetite in carbonatite, as shown by the presence of ilmenite lamellae. The evidence is clear that the magnetites in the reaction bands were produced from titanomagnetite in the jacupirangite by exsolution of ilmenite. However, as concluded in connection with Figure 9, there are other chemical reactions involved, and we have insufficient evidence to work them out in detail. More information is required about the range of titanomagnetite compositions in jacupirangite, and the intermediate stages of the reaction between jacupirangite and carbonatite.

Metasomatic processes involved in the formation of the banded rocks produce magnetites in the silicate bands only, which do not correspond closely in composition to the magnetites in the associated carbonatites. Therefore, we see no evidence supporting extrapolation of metasomatic processes in the reaction bands to the origin of carbonatite intrusions as a whole.

Discussion

The field evidence that the carbonatite plug at Jacupiranga is made up of not two (Melcher, 1966)

but five intrusions (Table 1), plus many dikes, indicates that the petrogenesis may be quite complex. The evidence from the magnetite compositions confirms that the five intrusions were not produced simply by a continuous process of differentiation.

The magnetites occupy a very limited range of compositions near Fe_3O_4 (Fig. 2), as do magnetites from other carbonatites (Fig. 10; Boctor and Svisero, 1978; Michell, 1979), but they are sufficiently sensitive to conditions of growth that the core compositions in each of the five intrusions can be distinguished on the basis of variations in MgO, FeO, Fe_2O_3, Al_2O_3, TiO_2, and MnO. Despite the limited range of compositions, it appears that magnetite crystals nucleated through most of the crystallization intervals of each carbonatite. The evidence for marginal resorption shown in textures and some zoning profiles (Figs. A1 through A5) indicates a change during the closing stages of crystallization.

There is good evidence from the magnetites that the oldest carbonatite, C_1, was derived from a magma somewhat different chemically from those producing intrusions C_2 through C_5. Furthermore, it appears from the magnetite core composition ranges and zoning that C_1 was not precipitated from a single, homogeneous batch of magma. The variations in magnetite compositions for the other carbonatite intrusions are simpler, and are consistent with precipitation of each from a single batch of magma. The formation of C_2 probably went to completion independently of the younger intrusions, C_3 through C_5. However, the ranges of core compositions of magnetites in C_3 through C_5 are consistent with their precipitation from three successive batches of magma which represent a continuum in time and magmatic evolution. Whether the magma precipitating C_3 (and perhaps subsequently C_4 and C_5) was separated from that precipitating C_2 early in the C_2 history, or whether a common parent yielded two successive magmas which independently precipitated carbonatites C_2 and then C_3, cannot yet be determined. Nor do the magnetites inform us whether the carbonatite magmas were derived from a silicate parent magma by crystallization differentiation, or by liquid immiscibility. More detailed investigation of the inclusions in magnetite and other minerals may yield information about the compositions of the magmas, and of the elements such as alkalis which are poorly represented in the carbonatites, presumably because the residual fluids escaped from the crystalline deposits and fenitized the country rocks.

These results from magnetite, a simple and commonly neglected mineral in carbonatities, illustrate a remarkable sensitivity to conditions of crystallization. When supplemented by the detailed studies of other minerals in the carbonatites, they will provide an even higher potential for unravelling petrogenesis.

Mitchell (1979) reviewed spinels in several rocks, and noted that spinel compositions in kimberlites, lamprophyres, and carbonatites all converge upon Fe_3O_4 (see Fig. 2). Mitchell (1978, 1979) and Boctor and Svisero (1978) emphasized that magnetite from Jacupiranga and other carbonatites differs markedly from spinel phases in kimberlites.

Mitchell (1979) presented a stimulating and incisive review of evidence to refute the "alleged kimberlite–carbonatite relationship", the commonly held view that kimberlites and carbonatites are genetically related. The marked difference in compositions of spinels from kimberlites and from carbonatites is important evidence in the refutation. He cited the experimental, field and petrographic observations demonstrating conclusively that kimberlite magma differentiates to carbonate-rich SiO_2-poor residua. He emphasized that although these rocks would be termed carbonatite according to the petrographic classification of Heinrich (1966), they have very different mineralogies, antecedents, and comagmatic rocks to the carbonatites of alkaline complexes.

Mitchell (1979) is, of course, correct to state that the carbonatites of Jacupiranga, and other associated with alkaline rock associations, have characteristics, origins and histories different from those of carbonatites derived from kimberlites. It is most unfortunate that the search for petrogenetic links between rocks of the two associations has led to confused petrogenetic speculations and misdirected exploration efforts for niobium and diamond (Mitchell, 1979), but we do not think that this is sufficient reason to terminate the intellectual exercise of tracing the links between kimberlites and carbonatites. There are two problems here, petrographic or semantic, and petrogenetic. Mitchell (1979) recommended that the carbonatites associated with kimberlites should be called "calcareous kimberlites" or "calcite-kimberlites", and he objected to the lax application of the term "carbonatitic" to the presumed interstitial carbonate-rich magma in the upper asthenosphere (Wyllie and

Huang, 1975). It is within the upper mantle that the petrogenetic links are joined. Kimberlites and "calcite-kimberlites", and alkaline complexes and carbonatites, are two of the diverse products from upper mantle processes which are influenced by CO_2 (Wyllie and Huang, 1976; Eggler, 1978; Wyllie, 1980). LeBas (1977, Fig. 24.1) presented a spectrum of ultramafic magmas from the mantle and their evolution along five derivatives stems, with kimberlites at one end, and carbonatites at the other.

Detailed studies of carbonatites and of carbonate-rich derivatives of kimberlites are a prerequisite for tracing their petrogenetic histories and that of their magmatic antecedents back towards their mantle source, and for eventual comprehension of why carbon in the upper mantle is conveyed to the surface in different tectonic environments as carbonatites, containing phosphorus, niobium, and rare earth elements, or as calcite-kimberlite associated with graphite or diamond.

Acknowledgments

We thank Serrana S/A de Mineracão, G. C. Melcher, and V. A. V. Girardi for making possible the field work of JCG, I. M. Steele for invaluable assistance with microprobe analyses and for the computer program to calculate Fe^{3+}, and J. V. Smith for assistance with the microprobe. Financial support was provided by Conselho Nacional de Desenvolvimento Científico e Tecnológico (CNPq) PROC 201.158/80 and PROC 40.1410/81, Fundação de Ampara à Pesquisa do Estado de São Paulo (FAPESP) PROC 80/470 and PROC 81/0168-8, and the Earth Science Division of the National Science Foundation Grants EAR 76-20410, and EAR 81-08599.

References

Amaral, G. (1978) Potassium–argon age studies on the Jacupiranga alkaline district, State of São Paulo, Brazil. Proceedings of the First International Symposium on Carbonatites, p. 297–302. Departamento Nacional da Producão Mineral. Brasilia.

Boctor, N. Z. and Svisero, D. P. (1978) Iron–titanium oxide and sulfide minerals in carbonatite from Jacupiranga, Brazil. Carnegie Institution of Washington Year Book, 77, 876–880.

Carmichael, I. S. E., Turner, F. J., and Verhoogen, J. (1974) Igneous Petrology. McGraw-Hill Book Company, New York.

Eckermann, H. von (1974) The chemistry and optical properties of some minerals of the Alnö alkaline rocks. Arkiv för Mineralogi och Geologi, 5, 93–210.

Eggler, D. H. (1978) The effect of CO_2 upon partial melting of peridotite in the system Na_2O–CaO–Al_2O_3–MgO–SiO_2–CO_2 to 35 kb, with an analysis of melting in a peridotite–H_2O–CO_2 system. American Journal of Science, 278, 305–343.

Gittins, J. (1978) Some observations on the present status of carbonatites studies. Proceedings of the First International Symposium on Carbonatites, p. 107–115. Departamento Nacional da Producão Mineral. Brasilia.

Gold, D. P. (1966) The minerals of the Oka carbonatite and alkaline complex, Oka, Quebec. Mineralogical Society of India, IMA Volume, 109–125.

Haggerty, S. E. (1976) Opaque mineral oxides in terrestrial igneous rocks. In D. Rumble, III, Ed., Oxide Minerals, p. Hg101–Hg300. Mineralogical Society of America.

Heinrich, E. Wm. (1966) The Geology of Carbonatites. Rand McNally and Company, Chicago.

Herz, N. (1977) Timing of spreading in the South Atlantic: information from Brazilian alkalic rocks. Geological Society of America Bulletin, 88, 101–112.

Irvine, T. N. (1965) Chromian spinel as a petrogenetic indicator. Part I. Theory. Canadian Journal of Earth Sciences, 2, 648–672.

Koster van Groos, A. F. and Wyllie, P. J. (1966) Liquid immiscibility in the system Na_2O–Al_2O_3–SiO_2–CO_2 at pressures up to 1 kilobar. American Journal of Science, 264, 234–255.

Koster van Groos, A. F. and Wyllie, P. J. (1973) Liquid immiscibility in the join $NaAlSi_3O_8$–$CaAlSi_2O_8$–Na_2CO_3–H_2O. American Journal of Science, 273, 465–487.

LeBas, M. J. (1977) Carbonatite–Nephelinite Volcanism. John Wiley and Sons, London.

Lindsley, D. H. (1976) Experimental studies of oxide minerals. In D. Rumble, III, Ed., Oxide Minerals, p. L61–L88. Mineralogical Society of America.

McMahon, B. M. and Haggerty, S. E. (1976) Oka carbonatite complex: oxide mineral zoning in mantle petrogenesis. Geological Society of America, Abstracts with Programs, 8, 1006.

McMahon, B. M. and Haggerty, S. E. (1979) The Oka carbonatite complex: magnetite compositions and the related role of titanium in pyrochlore. In F. R. Boyd and H. O. A. Meyer, Eds., Kimberlites, Diatremes and Diamonds: Their Geology, Petrology, and Geochemistry, p. 382–392. American Geophysical Union.

Melcher, G. C. (1966) The carbonatites of Jacupiranga, São Paulo, Brazil. In O. F. Tuttle and J. Gittins, Eds., Carbonatites, p. 169–181. John Wiley and Sons, New York.

Mitchell, R. H. (1978) Manganoan magnesian ilmenite and titanian clinohumite from the Jacupiranga carbonatite, São Paulo, Brazil. American Mineralogist, 63, 544–547.

Mitchell, R. H. (1979) The alleged kimberlite–carbonatite relationship: additional contrary mineralogical evidence. American Journal of Science, 279, 570–589.

Prins, P. (1972) Composition of magnetite from carbonatites. Lithos, 5, 227–240.

Reed, S. J. B. (1973) Principles of X-ray generation and quantitative analysis with the electron microprobe. In C. A. Andersen, Ed., Microprobe Analysis, p. 53–81. John Wiley and Sons, New York.

Secher, K. and Larsen, L. M. (1980) Geology and mineralogy of the Sarfartôq carbonatite complex, southern West Greenland. Lithos, 13, 199–212.

Steele, I. M., Bishop, F. C., Smith, J. V., and Windley, B. F. (1977) The Fiskenaesset complex, West Greenland, Part III. Chemistry of silicate and oxide minerals from oxide bearing rocks, mostly from Qeqertarssuatsiaq. Grønlands Geologiske Undersøgelse, 124, 1–38.

Tuttle, O. F. and Gittins, J. (1966) Carbonatites. John Wiley and Sons, New York.

Ulbrich, H. H. G. J. and Gomes, C. B. (1981) Alkaline rocks from continental Brazil: a review. Earth Science Reviews, 17, 135–154.

Wyllie, P. J. (1978) Silicate–carbonate systems with bearing on the origin and crystallization of carbonatites. Proceedings of

the First International Symposium on Carbonatites, p. 61–68. Departamento Nacional da Producão Mineral. Brasilia.
Wyllie, P. J. (1980) The origin of kimberlite. Journal of Geophysical Research, 85, B12, 6902–6910.
Wyllie, P. J. and Huang, W. L. (1975) Periodotite, kimberlite, and carbonatite explained in the system CaO–MgO–SiO_2–CO_2. Geology, 3, 621–624.
Wyllie, P. J. and Huang, W. L. (1976) Carbonation and melting reactions in the system CaO–MgO–SiO_2–CO_2 at mantle pressures with geophysical and petrological applications. Contributions to Mineralogy and Petrology, 54, 79–107.
Wyllie, P. J. and Tuttle, O. F. (1960) The system CaO–CO_2–H_2O and the origin of carbonatites. Journal of Petrology, 1, 1–46.

Manuscript received, February 11, 1982;
accepted for publication, September 7, 1982.

Appendix

This Appendix contains additional descriptive material and figures, which are cited in the preceding text.

Analytical procedure

Standards used for the electron microprobe analyses were diopside glass (for Ca, Si, and Mg), Fe metal (for Fe), synthetic rutile (for Ti), synthetic enstatite with 10% Al_2O_3 (for Al), and synthetic glass with 1 wt.% MnO (for Mn). The amount of Fe occurring as Fe^{3+} was calculated following the assumptions made by Steele *et al.* (1977).

The carbonatites are heterogeneous rocks, and many analyses were completed in an attempt to represent the average compositions of magnetites, as well as the ranges of zoning in each carbonatite. For each carbonatite sample analyzed, three to four magnetites were selected, and four to six points were analyzed in each mineral, including points in the core and rim regions (Table 2). Separate averages were calculated for core and rim determinations in each rock sample. In addition to this, details of the zoning were determined by analyzing a series of points across selected magnetite grains (each point is a single analysis).

The magnetites from the reaction rock with exsolved ilmenite lamellae had irregular form and no regular pattern of variation in composition. Therefore, average values for core and rim were not obtained. The values presented in Table 3 are the average of all data for each rock sample; the individual analyses cluster fairly closely around these values.

The magnetite intergrowth with sulfide occurred in very small patches, and only a few points could be analyzed. These points showed little variation in chemical composition. Averages for each magnetite intergrowth are given in Table 3.

Two crystals of magnetite from the jacupirangite were analyzed, one zoned (core and rim analyses), and another without zoning. Several point analyses were performed near the ilmenite lamellae, and the result obtained for a point nearest to one lamella is shown in Table 3.

Individual zoned crystals

Electron microprobe traverses across individual minerals from each of the five intrusions are presented in Figures A1 through A5. The traverses extend either from rim to rim passing through the centers of the mineral sections, or from core to rim. The horizontal distance scale varies from one mineral section to another. The vertical axis represents a constant scale in weight per cent of oxide, but for graphical convenience and to facilitate comparison of oxide variations, the profile for each oxide plotted is arbitrarily located with respect to the vertical scale. The absolute values for each figure are given at one end in weight per cent.

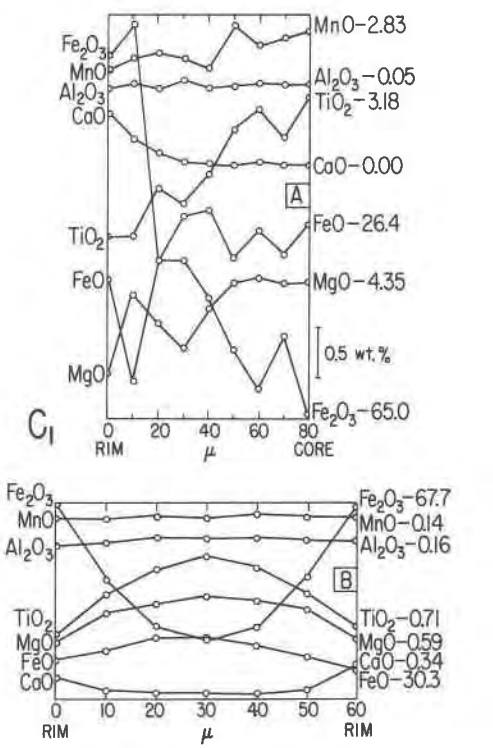

Fig. A1. Electron microprobe profiles for magnetites of the C_1 sovite. Each point represents a single analysis. These data are not tabulated.

Figure A1B, for carbonatite C_1, illustrates simple, regular and symmetrical zoning from core to rim. The other profiles in Figures A1 through A5 show broadly similar trends, but there are irregularities and reversals compared with the trends in Figure A1B. In general, the rate of chemical variation increases toward the rims of the minerals. These profiles provide information

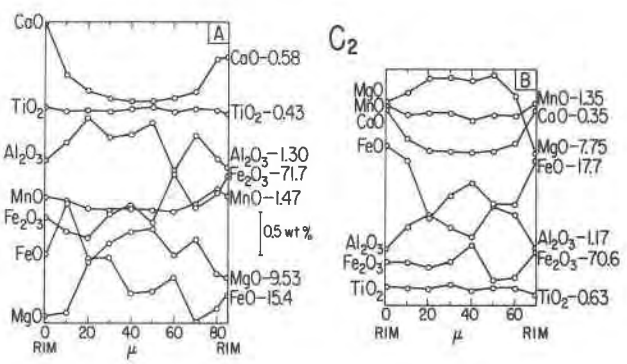

Fig. A2. Electron microprobe profiled for magnetites of the C_2 dolomitic sovite.

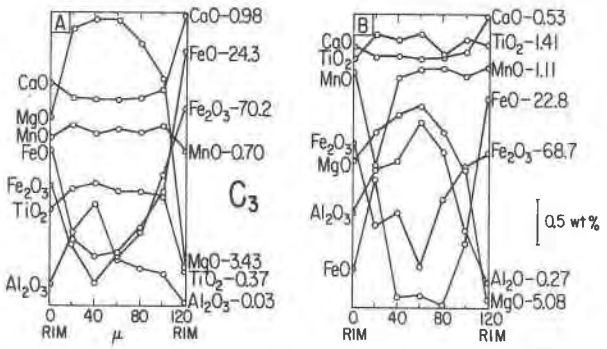

Fig. A3. Electron microprobe profiles for magnetites of the C_3 sovite.

about the sympathetic and antipathetic variations of trivalent and tetravalent cations in relation to the divalent cations, which determine the most important end-member components present, and their distribution in the zoned minerals.

The profiles in Figure A1 for magnetites in C_1 illustrate antipathetic behavior of TiO_2 and Fe_2O_3, indicating a variation from core to rim in the ulvospinel-magnetite solid solution series, with fairly constant Al_2O_3. In contrast, Figure A2 shows fairly constant TiO_2 for magnetites from carbonatite C_2, with antipathetic behavior between Al_2O_3 and Fe_2O_3. A similar relationship exists between Al_2O_3 and Fe_2O_3 for magnetites in C_3 (Figure A3), but there is in addition some variation in TiO_2. The zoning in the examples from C_4 in Figure A4 shows variations similar to those in C_3. The single example for C_5 in Figure A5 also shows antipathetic behavior between Al_2O_3 and Fe_2O_3, with little change in TiO_2. Despite the repetition of zoning patterns from magnetites in the different intrusions, it is evident that there are differences in composition between the magnetites; note, for example, the values for MgO and TiO_2 in the profiles.

Core compositions and ranges of zoning

Figures A6 and A7 show projections of mineral compositions from the spinel prism of Figure 2, as described in the text for Figures 4 and 5. The analyses are projected onto a vertical section through the prism in Figure A6, and onto the rear face of the prism in Figure A7. The range of values depicted for one of the C_2 analyses is representative of the ranges from which the average values were derived.

In Figures 4B, A6B and A7, the average core composition of each magnetite is connected to the average composition of its rim (Table 2). Every pair of analyses has a component of increasing FeO/(FeO+MgO) from its core to rim, indicating that this ratio has a time relevance, which is consistent with the relationship illustrated for the cores of magnetites in C_2, C_3, C_4, C_5 in Figure 3.

The average magnetite core compositions for each carbonatite intrusion are enclosed by lines which were drawn with two criteria: (1) to fit the boundaries around the points as closely as possible, and (2) to draw the boundaries so that there were no reversals in direction with respect to FeO/(FeO+MgO). The results depict fairly narrow chemical bands for the core compositions in each of the intrusions and, although additional analyses could broaden the areas, and fill in the re-entrant angles, the results indicate that the chemical variation trends for the core magnetites in each of the five intrusions are distinct from each other. The separation of C_3, C_4, and C_5 was already evident from Figure 3. Although C_1 overlaps with the other four intrusions in Figure 3, the trend is distinct from that of the others in Figures 4A and 5, and distinguishable in Figure A6A. The trend of C_4 obviously differs from that of C_2 in Figures 4A and 5, although the C_2 composition boundary just reaches the C_4 boundary. The trend of C_2 differs from that of C_3 in Figures 4A, A6A, and 5, but the separation is not convincing. However, the separation of core compositions from C_2 and C_3 is confirmed in Figure 6, where the Mn content is plotted against the Mg content. Figure 6 also separates the magnetite cores of C_1 from those of C_2 and C_3.

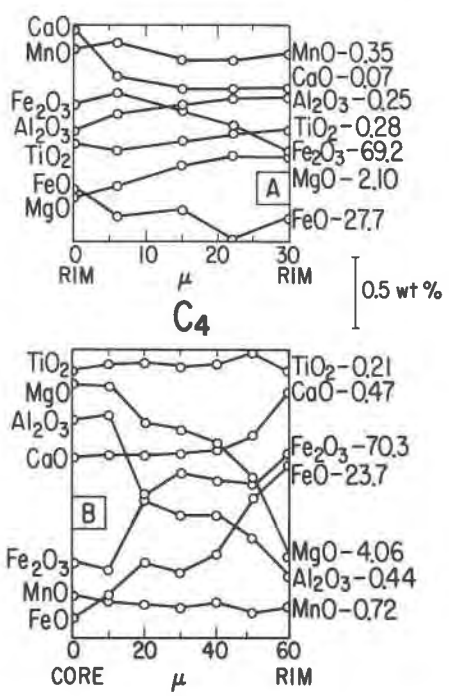

Fig. A4. Electron microprobe profiles for magnetites of the C_4 sovite.

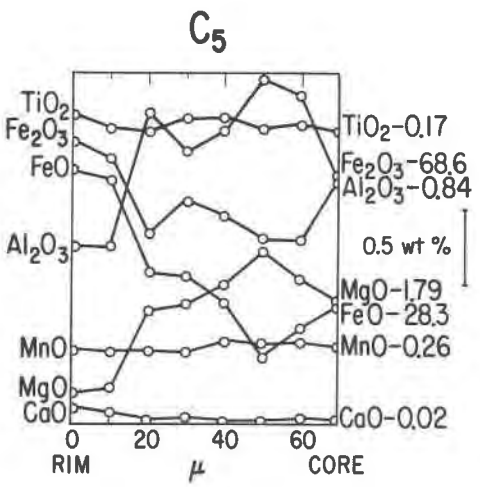

Fig. A5. Electron microprobe profile for a magnetite of the C_5 rauhaugite.

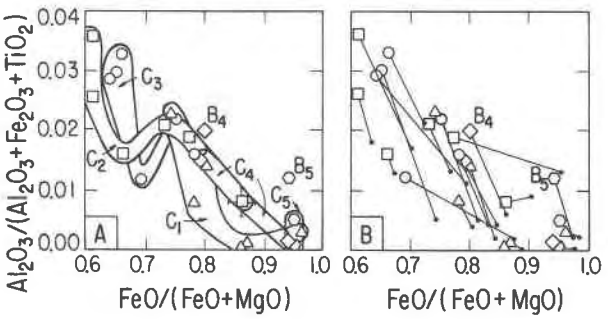

Fig. A6. Average core and rim compositions of magnetites (Table 2) in projections from the spinel prism (Figure 2). A representative range of values is shown for one of the points. A. Core compositions. See Figure 3 for symbols. B. The core compositions connected by lines to corresponding rim compositions (dots) showing zoning trends.

The magnetites in beforsite dikes B_4 and B_5, respectively, have FeO/(FeO+MgO) equal to the low end of the range for C_4, and equal to that in C_5 (Fig. A6). They have the same values for $Fe_2O_3/(Fe_2O_3+TiO_2)$ as magnetites in C_4 and C_5, distinctly higher $Al_2O_3/(Al_2O_3+Fe_2O_3+TiO_2)$ and $Al_2O_3/(Al_2O_3+TiO_2)$, and slightly higher MnO (Figs. 4, 5, 6, and A6A).

Figure A6B illustrates a steady decrease in Al_2O_3 with decreasing MgO from cores to rims, with only one exception. This trend is consistent with the broad trend for the magnetite core compositions in Figure A6A.

The main zoning illustrated in Figure A7 (see Fig. 5) is directed towards the lower right-hand corner, representing the ulvospinel composition, with Al_2O_3 decreasing relative to TiO_2. This is also the dominant trend for the magnetite cores in Figure 5. However, four zoning lines reverse this trend. The zoning illustrated in Figure A7 is not a result of substitutions between Al-spinels (top of prism in Figure 2) and Ti-spinels (rear edge of the prism), but a consequence of the more rapid decrease of Al than Ti from core to rim (except for a few C_1 magnetites). This is evident if Ti is plotted against Al.

The progressive decrease in Mn contents of core magnetites with decreasing Mg content illustrated in Figure 6 is accompanied by a progressive change in the slopes of the zoning lines as shown in Figure A8. A 1:1 replacement line is drawn as a basis for comparison. For magnetites with the highest Mg contents, two of the zoning lines are consistent with the 1:1 substitution. However, with decreasing Mg content, the core compositions exhibit a broad trend converging toward the origin, and the zoning lines change direction fairly regularly until they, too, are directed towards the origin. This illustrates a change in zoning, from enrichment in Mn towards the rims for high-Mg magnetites, to depletion in Mn towards the rims for low-Mg magnetites. Note the three exceptions for high-Mg magnetites. Small marginal variations in MnO contents can be seen in the zoning profiles of Figures A1A, A2, and A3.

Magnetites from special locations

The three magnetites from jacupirangite plotted in Figure 8A define a straight line which extrapolates to the magnetites in the reaction bands from C_5 and C_1. The zoning in a magnetite from jacupirangite is parallel to the same line. The line is inclined, consistent with the anticipated decrease in MgO as ilmenite is exsolved from magnetite (Lindsley, 1976). The magnetite from the reaction rock in C_3 contains more MgO than that in the jacupirangite analyzed, and it departs significantly from the reaction trend indicated by the dashed line. A similar relationship is exhibited in Figure 8B. Extrapolation of the trend indicated by the three jacupirangite magnetites, and the zoning, reaches the magnetites in the reaction rocks from C_1 and C_5, but that from C_3 is separated from the others by its high MgO content.

Figure 9 shows the relationship between Mn and Mg. The magnetites from the jacupirangite establish a line, but extrapolation of the line does not lead to the magnetites in the reaction bands. These plot on a subparallel line following the trend of magnetites in the carbonatites. As the line defined by the jacupirangite magnetites represents the depletion of Ti due to exsolution of ilmenite, this sub-parallel line indicates that although the reaction rock magnetites may be derived from the jacupirangite magnetites, as indicated above, they are not produced by simple exsolution of ilmenite.

Comparison with previous results from the Jacupiranga carbonatite

In Figure 10, one of the magnetites reported by Boctor and Svisero plots in the C_2 range and the other two plot near the C_1 range. Of the two that plot near the C_1 magnetites, one is from olivine sovite, and the other is exsolved magnetite from phlogopite sovite. Some of the C_1 sovites are very rich in olivine, but we found no exsolved magnetite in our samples. In one of our C_1

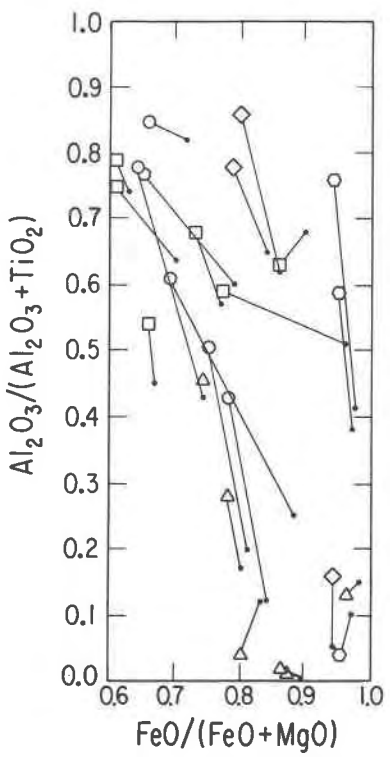

Fig. A7. Average core and rim compositions of magnetites plotted as in Figure 5. For symbols see Figure 3.

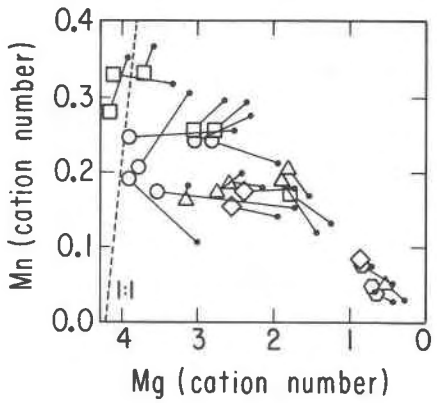

Fig. A8. Average core and rim compositions of magnetites plotted as in Figure 6. The dashed line represents 1:1 replacement. For symbols see Figure 3.

samples, the magnetite contains inclusions of ilmenite, but not exsolution lamellae. Boctor and Svisero plotted their results in a graph of Ti/(Ti+Al+Cr) against $Fe^{2+}/(Fe^{2+}+Mg)$. As Cr is present at very low levels, this plot is similar to our Figure 5. Their olivine-sovite magnetites correspond to our C_1 magnetites in Figure 5, and their phlogopite-sovite magnetites may correspond either to C_2 or to C_3 magnetites. Their exsolved magnetites correspond to the C_4 magnetites in Figure 5. The plot of MnO against MgO presented by Boctor and Svisero coincides with our results (Fig. 6), but our magnetites occupy a wider composition range. Our magnetites may contain almost 10 wt.% MgO (Table 2), while their highest MgO content is about 7 wt.%.

One of Mitchell's (1978) magnetite analyses with exsolved ilmenite lamellae plots near C_1 magnetites in Figure 10A, but the other two do not correspond to any of our ranges. The three analyses together in Figure 10B fit closest to the C_4 range. In Figure 5, they occupy the C_4 range, just as the exsolved magnetites of Boctor and Svisero did. We found no exsolved magnetites in our samples from C_4. However, C_4 is the only carbonatite of the five intrusions containing elongated subhedral crystals of ilmenite of primary origin (Gaspar and Wyllie, manuscript in preparation).

Comparison with magnetites from other carbonatites

Note in Figure 10 that the magnetites from three of the four additional localities have FeO/(FeO+MgO) greater than 0.9, and only two analyses from Oka have lower values, near 0.81. In contrast, as shown in Figure 3, more than half of the analyzed magnetites in the carbonatites of Jacupiranga have cores with FeO/(FeO+MgO) between 0.6 and 0.8; C_3 has none with values greater than 0.8; only four analyses from C_1, C_4, and C_5 have values greater than 0.9; and only intrusion C_5 is not represented by analyses with values less than 0.9.

The magnetites from Oka have FeO/(FeO+MgO) with values either near 0.81, or near 0.95. One of the magnetites is within the C_1 range, but the other three have lower $Fe_2O_3/(Fe_2O_3+TiO_2)$ and higher $Al_2O_3(Al_2O_3+Fe_2O_3+TiO_2)$ values than the Jacupiranga magnetites, for corresponding FeO/(FeO+MgO).

The two magnetites from Alnö, with FeO/(FeO+MgO) just above 0.9, are displaced from the Jacupiranga magnetites in the same way as the Oka magnetites. The single analysis from Sarfartôq is similarly displaced in Figure 10A, with an extreme range of zoning towards the top right-hand corner, whereas in Figure 10B it plots close to the C_5 area. Most of the magnetites from African carbonatites have the highest values of FeO/(FeO+MgO) plotted. Those without exsolved ilmenite correspond most nearly to the areas for C_5 and the end of C_1, with one exception in Figure 10B which is displaced to a position near magnetites from Oka and Alnö. The higher TiO_2 content of those with exsolved ilmenite is indicated by their lower positions in Figure 10A, similar to the Alnö and most of the Oka magnetites, although the latter are also characterized by higher Al_2O_3 than the Jacupiranga and African magnetites (with one exception). The magnetites in Figure 10B with high Al_2O_3 are similar to the magnetites from the Jacupiranga dikes B_4 and B_5 in Figures A6A and 4, and to the contact rocks B and S in Figure 8B. There is nothing noteworthy about the positions of magnetites from the other carbonatites when plotted in Figure 5.

Boctor and Svisero (1978) plotted MnO against MgO for the carbonatite magnetites, and their results for Jacupiranga and African carbonatites are similar to results plotted in Figure 6. The Oka magnetites are distinguished by their very much higher MnO content, ranging from 2–12%. All values of MnO for the Jacupiranga carbonatites are less than 2%, and commonly less than 1% (Tables 2 and 3).